Supporting Information

Slater 10.1073/pnas.1403666111

SI Text

Phylogenetic Analysis

Morphological characters and their associated states are provided at the end of this section. Figs. S1 and S2 show the maximum clade credibility trees derived from a topology-only analysis and a simultaneous analysis of topology and divergence times, respectively.

Estimating Transition Rates Among Dietary Regimes

Fitting Markov models to the dietary regime data over 500 trees sampled from the Bayesian PP distribution revealed that a symmetrical model was most preferred. Table S1 shows the median transition rate estimates for each model, along with their ln(likelihoods), Akaike information criterion (AIC) scores, and AICcWs. The symmetrical model implies that forward and backward transition rates are identical between a given pair of states but differ among pairs of states. Although this model received the most support (median AICcW = 0.69), an all rates different model, where rates were free to vary for all transitions, received a moderate amount of relative support (median AICcW = 0.3).

To account better for uncertainty in model choice and parameter estimation, I computed model-averaged transition rates (Q) from parameter estimates for the 500 sampled trees. A model-averaged rate matrix is given in Table S2 and illustrated graphically in Fig. S5. The main effect of averaging over all three models is to decrease the rate of transitions from hypercarnivory into mesocarnivory (Q_{12} = 0.031) relative to the reverse (Q_{21} = 0.053). This result is intuitive, given that increasing adaptation to hypercarnivory has been viewed as a macroevolutionary ratchet that prevents reversion to more generalized diets and increases extinction risk (1).

Simulation Tests

Fitting OU models to comparative data requires that each terminal taxon in the tree, as well as each internal edge, is assigned to a particular macroevolutionary regime [2–4, but see ref. 5]. Extant species are typically assigned to a particular regime based on direct observation. For example, species can be assigned to dietary regimes for a subsequent analysis of dental evolution based on feeding observations taken from wild populations. For extinct taxa, ecology cannot be directly observed and must instead be inferred from fossilized remains. Circularity can arise, however, when the trait(s) used to classify species are the same as, or are correlated with, the trait(s) of macroevolutionary interest. This circularity need not be the case if an independent regime is imposed, for example, evolution before and after some temporally constrained event (2, 6, 7).

Arguably, we are often more interested in understanding whether trait evolution within a given clade is guided by selection toward distinct but temporally coincident adaptive peaks than by temporally distinct peaks. In such cases, an a priori classification method, such as discriminant analysis, must be used to classify species for which ecology is not known and cannot be observed via indirect means, such as fossilized stomach contents. In the best-case scenario, we might have a set of traits, for example, craniodental variables, that can be used to classify species to an evolutionary regime and a second set of traits, for example, postcranial metrics, that we wish to model according to the regimes previously inferred. This scenario is a best-case scenario because the classification variables are, by most standards, independent of the variables of macroevolutionary interest. Correlations may exist, but limbs are developmentally distinct from skulls and teeth, and so circularity is not implied. In the worst-case scenario, only one trait is available to classify species, and it happens to be the same one that we are interested in modeling. In this case, a circularity is implied; by classifying species based on the trait of interest, we would appear to bias ourselves toward finding support for evolutionary models that allow for distinct trait means according to ecology.

My discriminant analyses were based on set of traits that did not include the traits of interest, although they each exhibit some degree of correlation with one of the traits (RLGA) among the extant species sampled (Fig. S6 and Table S3). An ordination of the first two discriminant functions shows that both are required to discriminate between canids with different diets, particularly between mesocarnivores and hypocarnivores but also, to some extent, between hypercarnivores and mesocarnivores (Fig. S7). Only the first discriminant function correlates with RLGA, however, mostly due to the large negative loading of the relative length of the m1 blade on this axis, and species with different diets overlap in RLGA values along both axes (Fig. S8).

I examined the effect of a worst-case scenario, as described above, on model selection via simulation. Using the time-calibrated canid tree with the highest log-likelihood (the "best" tree; Fig. 1), I simulated 500 sets of trait data under a time-homogeneous, single-rate BM model. I used the maximum likelihood estimate (MLE) of σ^2 in all simulations, with no optimal trait values or attraction parameters. For each replicate, I then assigned species to one of three evolutionary regimes based on their simulated trait values by dividing the distribution of simulated trait values at the 0.33 and 0.66 quantiles. I then compared the fit of a time-homogeneous, single-rate BM model with the fit of a multipeak OU model with regimes determined according to species' trait values, as implemented in OUwie (4). I assessed model fit using small AICcWs.

The OU model was strongly preferred over the BM model for all simulated datasets (mean AICcW = 0.99, range = 0.99–1; Fig. S9). A false-positive rate of 100% is clearly a nonoptimal outcome and implies that support for OU models where terminals have been classified based on the trait being analyzed should be viewed with skepticism.

Further dissection of the results revealed a significant positive relationship between the estimated number of regime shifts in the simulated data and the MLEs of the α-parameter for the fitted OU model (Fig. S10). This result suggests a predictive test, where BM could be viewed as an insufficient model to explain the accumulation of morphological variation within and among dietary regimes if the MLE of α from the empirical dataset is greater than the MLE of α predicted by simulation, given an inferred number of transitions. For RLGA on the best canid tree (Fig. 1), the estimated number of transitions between dietary regimes is 24, a relatively but not significantly (P = 0.16; Fig. S11) low number compared with the BM simulations. The MLE of α is 0.3352. This model implies very rapid rates of adaptation in RLGA ($t_{1/2}$ = 2.1 My). However, the predicted value of α for 24 dietary regime transitions under BM is 0.3346 (95% prediction interval = 0.25–0.41; Fig. S10). If we had classified canids to dietary regimes on the basis of RLGA values alone, there would clearly be a basis for rejecting, or at least being skeptical of, the best-fitting OU model.

Morphological Characters

Abbreviations: C, canine; I, incisors; M, molar; P, premolar. Uppercase refers to upper dentition, and lowercase refers to lower dentition.

1. Basal cusps on I1-2: absent (0); present (1) (8)
2. Size of I3: unenlarged relative to I1-2 (0); enlarged relative to I1-2 (1); greatly enlarged, possibly caniniform (2) (8–10)
3. Incisor row: curved, parabolic (0); straight line (1) (9)
4. I3 lateral cusps: I3 without lateral cusps (0); I3 with one lateral cusp (1); I3 with two lateral cusps (2); I3 with three lateral cusps (3) (9)
5. I1-3 medial cusps: present (0); absent on I3 only (1); weak or absent on I1-2 (2) (10)
6. c1 lateral groove: absent (0); present (1) (9)
7. Recurved c1: absent (0); present (1) (9)
8. Canine shape: long, slender (0); short, robust (1) (10)
9. Width of premolars: premolars not widened (0); premolars widened (1); premolars very wide and robust (2), premolars narrowed and slender (3) (8–10)
10. Premolar diastemata: closed premolar row (0); premolars separated by diastemata (1) (9, 10)
11. Anterior cingular premolar cusps: present on p2–4 (0); weak to absent on p2–4 (1); present only on p4 (2) (10)
12. Premolar crown height: premolars normal crown height (0); anterior premolars low crowned (1); high crowned (2) (9, 10)
13. Premolar length: short (0); elongate (1) (10)
14. P1: present (0); absent (1) (8)
15. p1: present (0); absent (1) (8, 9)
16. p3 posterior accessory cuspids: absent (0); present, moderately developed (1); present, enlarged (2) (8–10)
17. Height of principal cusp of p3 vs. p2, p4: forms ascending series or at same height (0); lies below p2 and p4 (1) (10)
18. Position of p3 crown base vs. crown base of p4: approximately same level as p4 when ramus is viewed laterally (0); crown base of p3 lies mostly below that of p4 (1) (10)
19. Second posterior accessory cusp of p3: absent (0); present (1) (9)
20. Relative size of p4: not greatly enlarged relative to p3 (0); greatly enlarged relative to p3 (1); further enlarged and reclined toward m1 (2) (8, 9)
21. p4 posterior accessory cusp position: located along midline of tooth (0); shifted laterally (1) (9)
22. p4 posterior accessory cusp size: moderate (0); enlarged (1); absent/lost (2) (9)
23. p4 second posterior accessory cusp: absent (0); present, lies between first posterior accessory cusp and cingulum (1); undifferentiated from posterior cingulum (2) (10)
24. p4 height relative to m1 paraconid: equals or exceeds m1 paraconid height (0); lower than m1 paranoid (1) (8, 9)
25. P4 protocone position: extends beyond anterior edge of paracone (0); medial to paracone (1) (8, 10)
26. P4 protocone size: unenlarged (0); enlarged (1); reduced (2); markedly reduced to small bulge with small root (3) (8–10)
27. P4 protocone and parastyle connection: protocone not connected to parastyle by a ridge (0); protocone connected to parastyle by a ridge (1) (9)
28. P4 parastyle: no P4 parastyle on anterior cingulum (0); parastyle originating from anterior cingulum separate from anterior ridge of paracone (1); strong ridge on anterior face of paracone (2); distinct parastyle as delineated by a notch on anterior ridge of paracone (3); parastyle prominently enlarged (4) (9)
29. P4 lingual cingulum or hypocone: internal cingulum weak or absent (0); cingulum thickened (1); cingulum raised to become hypocone (2) (9)
30. P4 shape: broad with strong anterior cingulum (0); narrow with weak anterior cingulum (1) (10)
31. M1 parastyle: large and salient (0); united with well-developed preparacrista (1); subdued, but remains united with preparacrista (2); preparacrista directed more anteriorly, lingual to parastyle (3) (8–10)
32. M1 paracone height: low, subequal to metacone (0); high and larger than metacone (1) (8–10)
33. M1 lingual cingulum: surrounds protocone anteriorly (0); posteriorly positioned and not surrounding protocone (1); anteriorly thickened (2) (8–10)
34. M1 labial cingulum at metacone: present at metacone (0); absent lateral to metacone (1) (9)
35. M1 labial cingulum at paracone: present at paracone (0); absent or subdued lateral to paracone (1) (9, 10)
36. M1 shape: anteroposteriorly short but transversely wide (0); subquadrate (1); longitudinally elongated (2) (9, 10)
37. M1 metaconule: weak or absent (0); present (1); large (2); metaconule split into two cusps (3) (9, 10)
38. M1 paraconule: weak or absent (0); distinct (1); enlarged (2) (9)
39. M1 posterior border shape: gently concave (0); sharply concave due to posterior extension of lingual cingulum (1) (9)
40. M1 hypocone: absent, lingual cingulum undifferentiated (0); hypocone present as swelling of posterior lingual cingulum (1); conical M1 hypocone present (2); conical M1 hypocone surrounded by cingulum (3) (9, 10)
41. M2 metacone: present, unreduced relative to paracone (0); reduced relative to paracone (1); extremely reduced or absent (2) (8, 9)
42. M2 hypocone: conical M2 hypocone absent (0); conical M2 hypocone present (1); conical M2 hypocone enlarged and posteriorly expanded (2) (9)
43. M2 metaconule and internal cingulum: metaconule and internal cingulum not connected (0); metaconule and internal cingulum connected by ridge (1); metaconule weak or absent (2) (9, 10)
44. M2 posterior cingulum: absent or weakly developed (0); present and well developed (1) (9)
45. M2 postprotocrista: present (0); incomplete or absent (1) (10)
46. M3: present (0); absent (1) (8)
47. m1 metaconid: present (0); unreduced, subequal to protoconid (1); present, reduced, almost vestigial (2); absent (3) (8, 10)
48. m1 protostylid: absent, weak ridge only (0); present, small (1); present, large, isolated from protoconid (2) (9, 10)
49. m1 anterior edge of paraconid: nearly linear and vertical (0); inclined posteriorly, may be curved (1) (10)
50. m1 trigonid elongation: m1 trigonid short (0); m1 trigonid elongated and open (1); m1 trigonid further shortened (2) (9)
51. m1 hypoconid form: hypoconid of m1 ridge-like (0); hypoconid of m1 conical (1) (8)
52. m1 entoconid form: poorly differentiated low crest on lingual border of talonid (0); discrete conical cusp (1) (9)
53. m1 talonid transverse cristid connecting hypoconid to entoconid: absent (0); present (1) (9)
54. m1 entoconulid: continuous with metaconid anteriorly or with small entoconulid between them (0); m1 entoconid deeply notched anteriorly, resulting in lingually open talonid (1); elevated, enlarged entoconulid anterior to entoconid (2) (9)
55. m1 talonid width: subequal with trigonid (0); wide relative to trigonoid (1); narrow relative to trigonid (2) (9)
56. m1 hypoconulid shelf: absent (0); present (1) (10)
57. m2 metaconid height: subequal in height with paraconid (0); shorter than paraconid (1); absent (2); much higher than protoconid (3) (8–10)

58. m1–2 selenodont: not selenodont (0); selenodont by development of crescentic labial talonid cusps (1) (9)
59. m2 size: unreduced/enlarged: smaller than m1 (0); enlarged relative to m1 (1); reduced in size relative to m1 (2) (8, 9)
60. m2 protostylid: protostylid absent (0); m2 protostylid present, small (1); m2 protostylid present, large (2) (9, 10)
61. m2 paraconid: present (0); weak or absent (1) (10)
62. m2 talonid length: talonid <90% trigonid (0); talonid >90% trigonid (1) (10)
63. m2 anterolabial cingulum: weak (0); well-developed, often reaching labial side of protocone (1) (10)
64. m3 trigonid cusps: two (0); single, centrally placed cusp (1); m3 absent (2) (8, 10)
65. m3 posterior shelf-like cingulum: absent (0); present (1) (10)
66. Rostrum length: mesocephalic (0); slightly dolichocephalic (1); extremely dolichocephalic, premolars widely spaced (2); relatively brachycephalic (3); extremely brachycephalic, premolars crowded (4) (8, 9)
67. Anterior palatine foramina length: short, posterior border lies at or anterior to posterior end of canine alveolus (0); long, posterior border lies posterior to canine alveolus (1) (10)
68. Palatine length: extends posterior to, or just anterior to, end of tooth row (0); extends beyond end of tooth row (1) (11)
69. Anterior process of frontal: smoothly curved frontal process (0); frontal process laterally pinched with sharp corner at its base (1) (8)
70. Nasal process of frontal: long (0); short (1) (10)
71. Premaxillary contact with frontal: premaxilla does not meet frontal, nasal, and maxilla in contact (0); premaxilla forms short contact with frontal, no nasal-maxilla contact (1); premaxilla forms broad contact with frontal (2) (9)
72. Nasal length: long, usually extending posteriorly beyond most posterior position of frontomaxillary suture (0); short, does not extend beyond frontomaxillary suture (1) (10)
73. Infraorbital foramen shape: rounded or oval shaped (0); compressed into a vertical slit (1) (8)
74. Elongation of orbital portion of skull: not elongated in middle section of skull (0); skull elongated, postorbital constriction situated well posterior of postorbital process (1) (8)
75. Foramen ovale and alisphenoid canal: separate (0); in common pit (1) (10)
76. Alisphenoid canal: present (0); absent (1) (12)
77. Frontal sinus: no frontal sinus, presence of a depression on dorsal surface of postorbital process (0); small frontal sinus that does not invade postorbital process or extend beyond postorbital constriction, depression may be retained (1); sinus invades postorbital process and may extend posteriorly to frontoparietal suture (2); sinus extends posteriorly beyond frontoparietal suture (3); sinus penetrates far back over top of entire braincase (4) (8–10)
78. Dorsal inflation of frontal sinus: flat forehead without dorsal inflation of sinus (0); small dome in forehead due to slight dorsal inflation (1); prominently domed forehead (2) (9)
79. Maxillojugal suture shape: obtuse (0); acute (1) (10)
80. Masseteric scar on zygomatic arch: masseteric scar wide and deep, particularly anteriorly, occupies >1/2 of lateral surface of zygomatic arch (0); masseteric scar narrow, restricted mostly to ventral face of arch and <1/3 depth of arch in lateral view (1) (9)
81. Orbital margin of zygomatic arch: laterally flared and everted (0); not laterally flared or everted (1) (9, 10)
82. Widest point of zygomatic arch: zygomatic arch gently curved laterally in dorsal view, widest point close to middle (0); widest point posteriorly shifted close to glenoid fossa, creating a more angled than arched appearance in dorsal view (1) (9)
83. Lateral expansion of zygomatic arches: unexpanded (0); laterally expanded (1) (8)
84. Zygomatic arch shape: nearly flat or moderately arched in lateral view (0); strongly dorsoventrally arched (1) (10)
85. Form of temporal crests: single sagittal crest formed by merging of temporal crests behind postorbital process (0); double crested, often lyrate, but with little or no reinforcement of crests (1); strong, widely separated and parallel temporal crests enclosing a longitudinal valley (2) (9)
86. Height of sagittal crest: sagittal crest low (0); sagittal crest high (1); sagittal crest very high (2) (9)
87. Sagittal crest profile: dorsally arched or straight (0); concave (1) (9)
88. Sagittal crest location: confined to parietal (0); extends on to frontal (1) (10)
89. Lambdoidal crest constriction: lambdoidal crest not constricted (0); nuchal portion of crest constricted, forming a rectangular plate (1) (9)
90. Postparietal foramen: present (0); absent (1) (10)
91. Dorsal exposure of cerebellum: significant exposure dorsoposteriorly between cerebrum and lambdoidal crest (0); completely overlapped by cerebrum, not exposed dorsoposteriorly (1) (10)
92. Supraoccipital shield form: rectangular or fan-shaped, inion not overhanging condyles (0); triangular in shape, inion often pointed and overhanging condyles (1) (9, 10)
93. Insertion for rectus capitis dorsalis muscle above occipital condyles: no fossae present, smooth surface (0); rounded fossae present (1) (8)
94. Suprameatal fossa: absent (0); presence of a small suprameatal fossa (1); suprameatal fossa present and enlarged (2) (8, 9)
95. Entotympanic bulla: unossified or absent (0); ossified and present (1) (8)
96. Bulla size: uninflated for canid type (0); bulla inflated (1); bulla hypertrophied (2); bulla shortened (3) (8, 9)
97. Internal carotid artery: intrabullar (transpromontorial) (0); extrabullar, between entotympanic and petrosal, and located dorsal to basioccipital-entotympanic suture (1); extrabullar, embedded within entotympanic, and located ventral to basioccipital-entotympanic suture (2) (8)
98. Promontorium shape: globular and isolated (0); medially and anteriorly expanded, in contact with surrounding bone (1) (8)
99. Ectotympanic ring: ectotympanic forms half-ring, dorsal roof of external auditory meatus formed by squamosal (0); ectotympanic ring complete, forms entire external auditory opening (1) (9)
100. Meatal tube: absence of tubular meatus (0); presence of a short tube (1); presence of an elongate tube (2) (9)
101. Direction of paraoccipital processes: posteriorly oriented and not fused with bulla (0); ventrally directed, not widely fused with bulla (1); ventrally directed, fused with bulla along entire length (2) (8–10)
102. Size of paraoccipital process: short and slender (0); elongate and robust (1); further hypertrophied and keeled posteriorly (2) (8–10)
103. Lateral expansion of paraoccipital process: no lateral expansion (0); laterally extended (1); further extension into a wide blade (2) (8, 10)
104. Posterior expansion of paraoccipital: no posterior extension (0); posteriorly extended (1); further extended, leading to development of a longitudinal plate (2) (8, 11)
105. Mastoid process form and size: small, crest-like (0); large, knob-like, inflated (1); prominently inflated beyond squamosal shelf (2); ventrally expanded (3); mastoid process very reduced, further receded under squamosal shelf (4) (8–10)

106. Lateral ridge of mastoid: absent (0); present (1) (9)
107. Postglenoid foramen and ectotympanic: postglenoid foramen enclosed posteriorly by ectotympanic (0); postglenoid foramen not enclosed posteriorly (1); ectotympanic extensively fused with postglenoid process (2) (8)
108. Optic foramen and anterior lacerate foramen: separate (0); in common pit (1) (10)
109. Medial pocket of angular process: absence of a pocket (0); presence of a deep medial pocket on angular process formed by lateral and dorsal extension of internal ridge (1) (8)
110. Angular process shape: attenuated, often with dorsal hook (0); shortened, blunt, deep (1) (8–10)
111. Relative size of fossa for superior ramus of medial pterygoideus muscle: small (0); fossa for superior ramus much larger than inferior (1) (10)
112. Subangular lobe of mandible: absent (0); present, rounded, smooth (1); present, sharply distinguished (2); present, dorsoventrally deep, angular (3) (9, 10)
113. Masseteric fossa ventral margin excavation: shallow (0); deeply excavated into ventral rim (1) (8)
114. Masseteric fossa ventral margin position: close to lower border of horizontal ramus (0); elevated, creating space between lower border of ramus and masseteric fossa (1) (9)
115. Masseteric fossa anterior margin: anterior margin of fossa not excavated (0); deeply excavated anteriorly (1) (9)
116. Shape of horizontal ramus: deep and strong (0); shallow and slender (1) (9, 10)
117. Symphyseal flange: ramus without flange (0); ramus with a symphyseal flange (1) (8)
118. Position of condyle: low (0); elevated above tooth row (1) (8)
119. Entepicondylar foramen of humerus: present (0); absent (1) (10)
120. Supratrochlear foramen of humerus: absent (0); present (1)
121. Metatarsal I: present with phalanges (0); reduced to rudiment, lacking phalanges (1) (10)
122. Radial-tibial ratio: <80% (0); 80–90% (1); >90% (2) (10)
123. Baculum size and shape: long, curved (0); short, straight (1) (8)

1. Van Valkenburgh B (1991) Iterative evolution of hypercarnivory in canids. *Paleobiology* 17(4):340–362.
2. Hansen TF (1997) Stabilizing selection and the comparative analysis of adaptation. *Evolution* 51(5):1341–1351.
3. Butler MA, King AA (2004) Phylogenetic comparative analysis: A modeling approach for adaptive evolution. *Am Nat* 164(6):683–695.
4. Beaulieu JM, Jhwueng DC, Boettiger C, O'Meara BC (2012) Modeling stabilizing selection: Expanding the Ornstein-Uhlenbeck model of adaptive evolution. *Evolution* 66(8):2369–2383.
5. Mahler DL, Ingram T, Revell LJ, Losos JB (2013) Exceptional convergence on the macroevolutionary landscape in island lizard radiations. *Science* 341(6143): 292–295.
6. Slater GJ (2013) Phylogenetic evidence for a shift in the mode of mammalian body size evolution at the Cretaceous-Palaeogene boundary. *Methods Ecol Evol* 4(8):734–744.
7. Benson RBJ, Frigot RA, Goswami A, Andres B, Butler RJ (2014) Competition and constraint drove Cope's rule in the evolution of giant flying reptiles. *Nat Commun* 5:3567.
8. Wang X (1994) Phylogenetic systematics of the Hesperocyoninae (Carnivora, Canidae). *Bulletin of the American Museum of Natural History* 221:1–207.
9. Wang X, Tedford RH, Taylor BE (1999) Phylogenetic systematics of the Borophaginae (Carnivora, Canidae). *Bulletin of the American Museum of Natural History* 243:1–391.
10. Tedford RH, Wang X, Taylor BE (2009) Phylogenetic systematics of the North American fossil Caninae (Carnivora: Canidae). *Bulletin of the American Museum of Natural History* 325:1–218.
11. Tedford RH, Wang X, Taylor BE (1995) Phylogeny of the Caninae (Carnivora, Canidae): The Living Taxa. *Am Mus Novit* 3146:1–37.
12. Wesley–Hunt GD, Flynn JJ (2005) Phylogeny of the Carnivora: Basal relationships among the carnivoramorphans, and assessment of the position of 'Miacoidea' relative to Carnivora. *J Syst Palaeontology* 3(1):1–28.

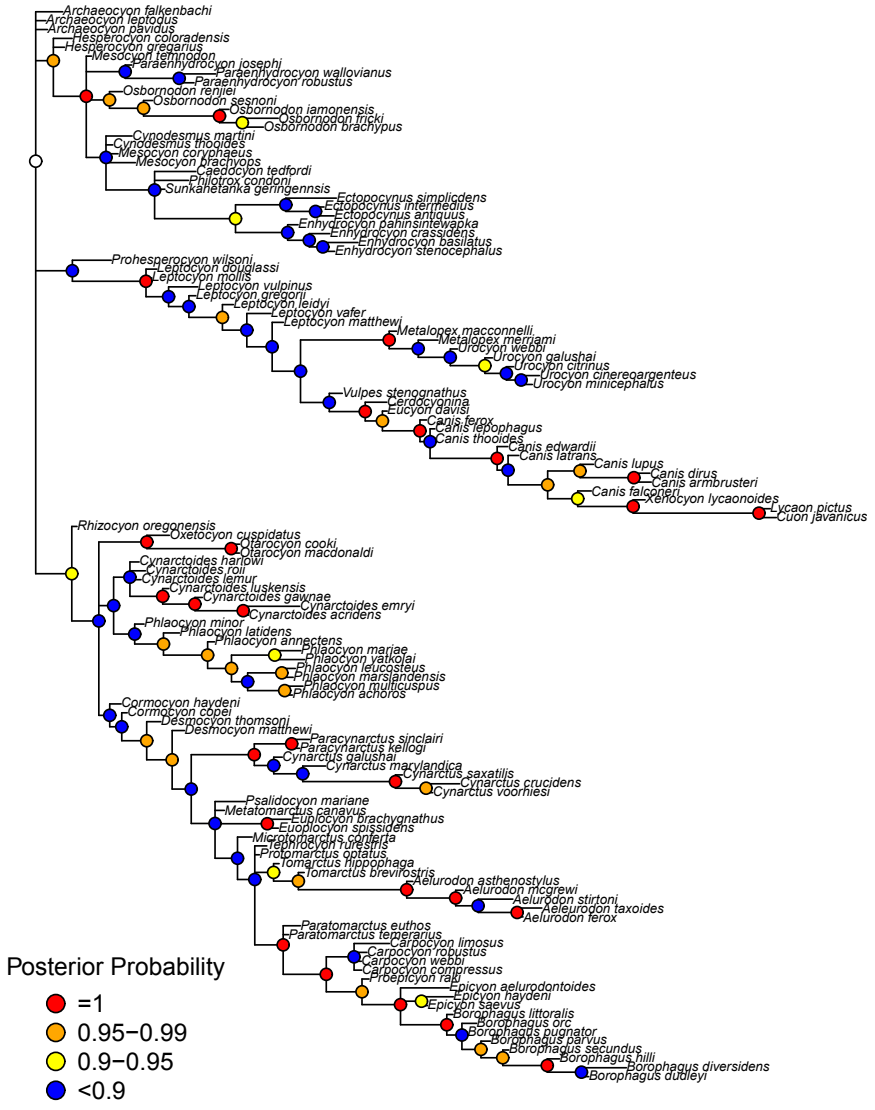

Fig. S1. Maximum clade credibility phylogram from a Bayesian analysis of 124 characters coded for 121 living and fossil canids plus one outgroup (removed).

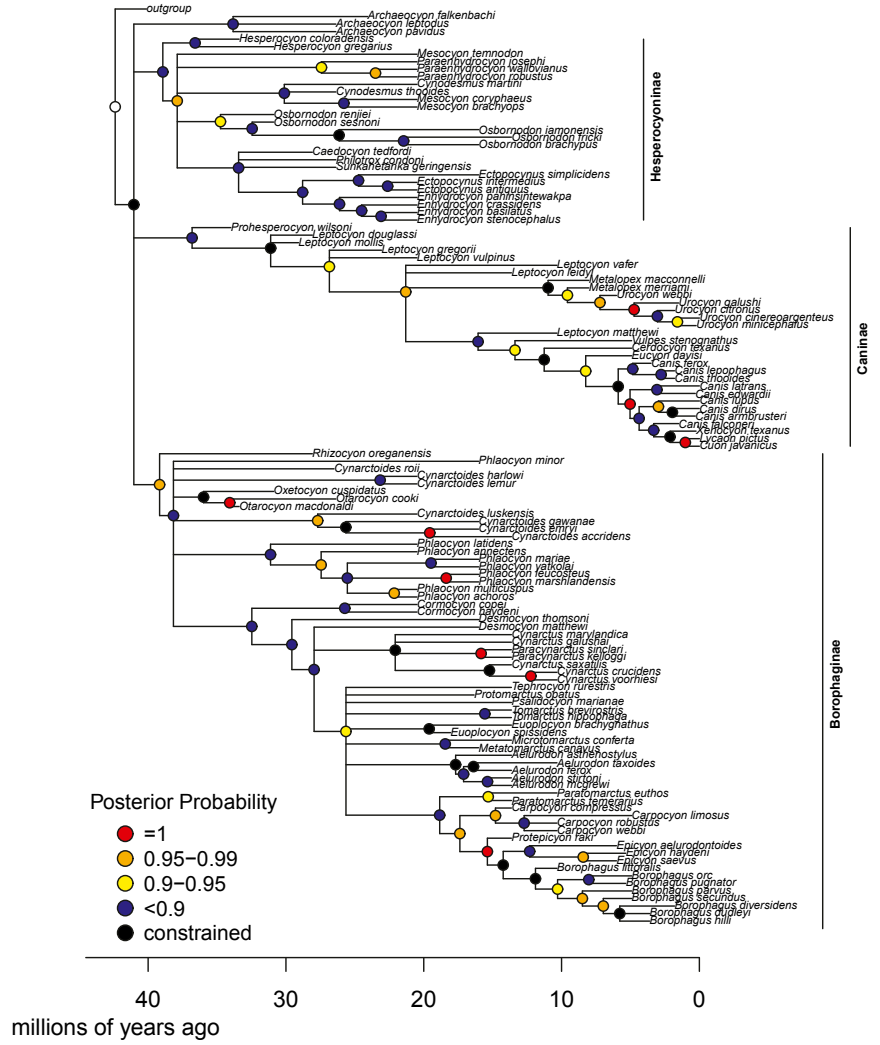

Fig. S2. Maximum clade credibility chronogram from a Bayesian tip dating analysis of 124 characters coded for 121 living and fossil canids plus one outgroup. Fossil species are plotted at their last appearance date. Divergence times are estimated under a relaxed, uncorrelated morphological clock, and therefore may occur after the first appearance date(s) in the fossil record of one or more daughter taxa. Constrained nodes are those nodes that were unambiguously supported in the topology analysis (PP = 1; Fig. S1), and where the oldest first appearance date of a descendant taxon was used to derive an informative node age prior.

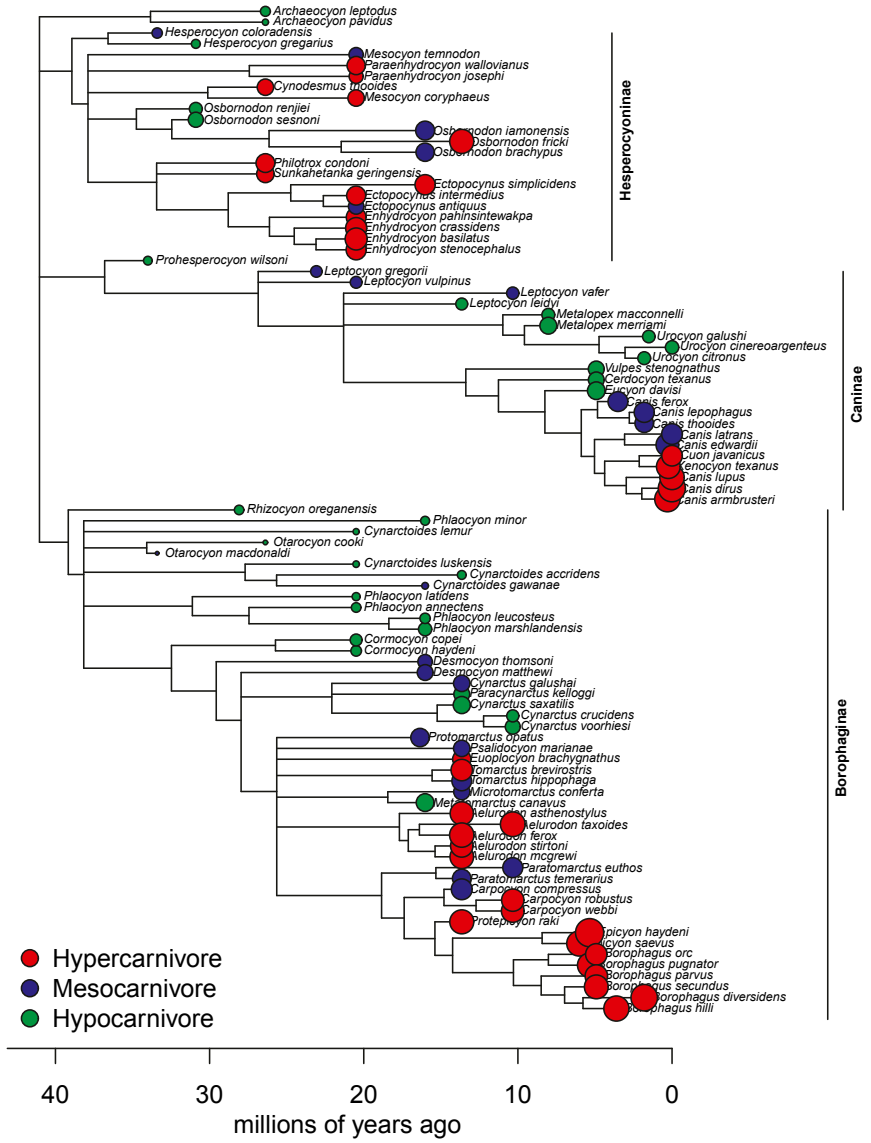

Fig. S3. Maximum clade credibility chronogram showing distribution of body size variation over canid subfamilies and through time. Circles are colored according to diet, with size scaled according to ln(mass).

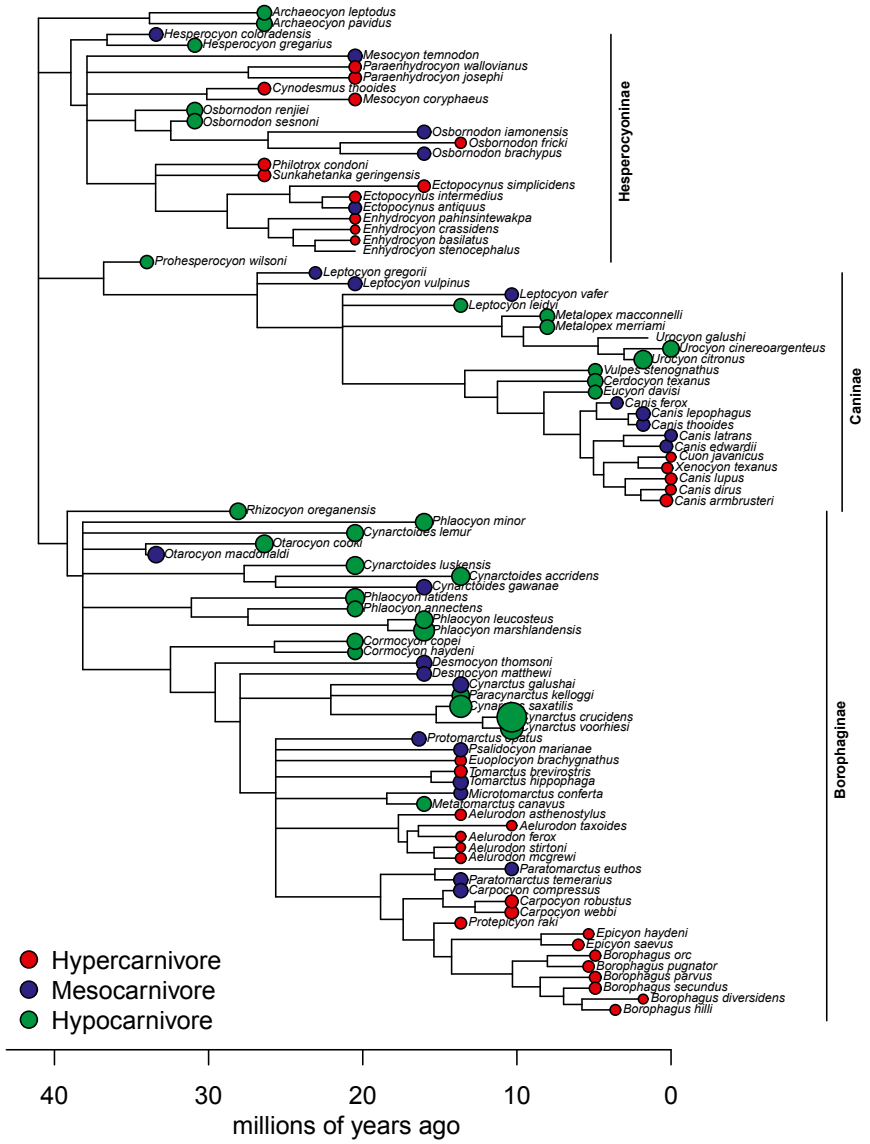

Fig. S4. Maximum clade credibility chronogram showing distribution of RLGA variation over canid subfamilies and through time. Circles are colored according to diet, with size scaled according to RLGA.

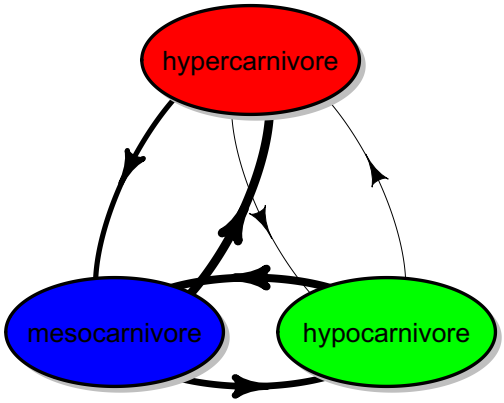

Fig. S5. Illustration of mean model-averaged rates between dietary states derived from 500 model fits. Although a symmetrical model is most strongly supported, model averaging of rates shows that transitions from hypercarnivore to mesocarnivore occur less frequently than transitions from mesocarnivore to hypercarnivore.

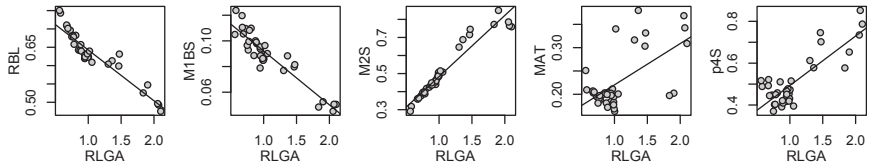

Fig. S6. Regression of the variables used to classify fossil canids to dietary groups on RLGA reveals significant correlations for all five traits (Table S3). MAT, moment arm of temporalis; M1BS, lower first molar blade size (relative to jaw length); M2S, relative size of upper second molar; p4S, shape of lower first premolar; RBL, relative length of the m1 blade.

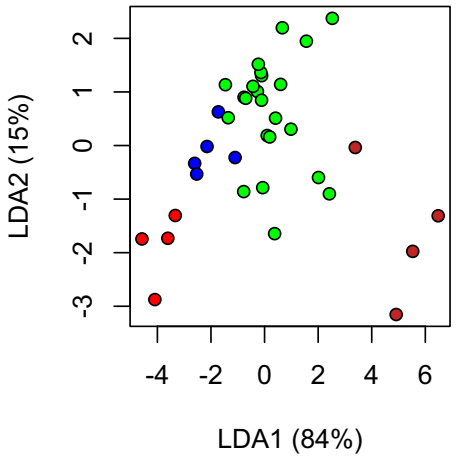

Fig. S7. Ordination of extant canids and procyonids on the first two discriminant functions. Colors correspond to dietary regimes: red, hypercarnivore; blue, mesocarnivore; green, hypocarnivore; brown, herbivore. Only procyonids and the red panda *Ailurus* are herbivorous. Note the substantial overlap of mesocarnivores and hypocarnivores on DF1 and of all groups on DF2. DF, discriminant function.

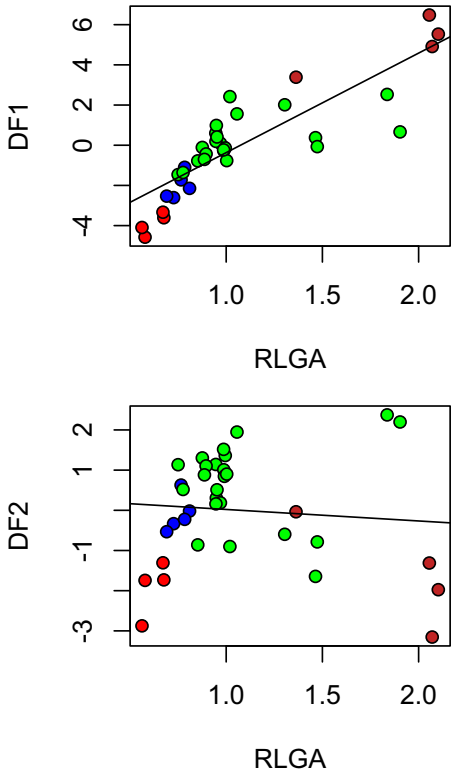

Fig. S8. Scatter plots showing the relationship between RLGA and scores on the first two DFs. The regression of DF1 on RLGA is significant ($R^2 = 0.72, P < 0.001$), but the regression of DF2 is not ($R^2 = -0.02, P = 0.6$).

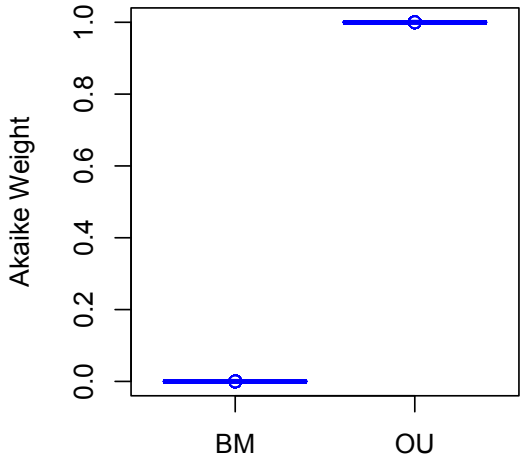

Fig. S9. AICcWs for BM and OU models fitted to 500 datasets simulated under BM and divided into three regimes based on trait values. The false-positive rate is 100%.

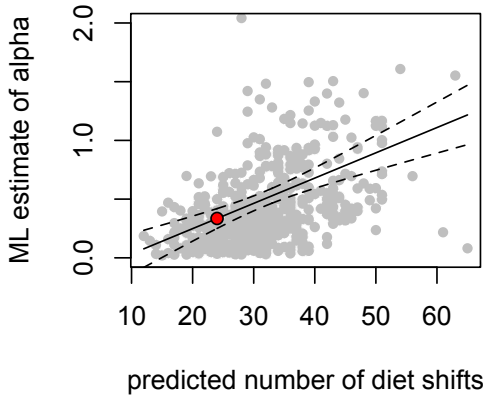

Fig. S10. There is a significant positive relationship ($R^2 = 0.06, P < 0.001$) between the predicted number of regime shifts in BM-simulated data and the MLE of the α-parameter of the OU model. However, the MLE of α from the empirical fossil canid dataset (red circle) falls within the 95% prediction envelope of this model, meaning that we cannot rule out BM in favor of OU in a worst-case scenario. The linear model is $\alpha = -0.18 + 0.215$.

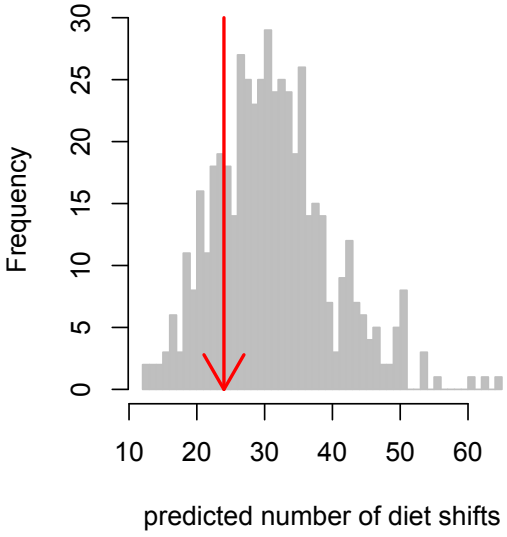

Fig. S11. Frequency distribution for the number of regime shifts (inferred via ancestral state estimation) implied in data simulated under BM and divided according to trait values. The number of regime shifts inferred for North American canids is shown by the red arrow; this number is not significantly different from the null distribution.

Table S1. Median transition rates and relative model support for discrete models of dietary evolution

Model	Q_{12}	Q_{13}	Q_{21}	Q_{23}	Q_{31}	Q_{32}	LnLk	AICc	AICcW
ER	0.0247	0.0247	0.0247	0.0247	0.0247	0.0247	−78.98	159.96	<0.01
SYMM	0.0412	0.0000	0.0412	0.0478	0.0000	0.0478	−72.07	150.14	0.69
ARD	0.0139	0.0000	0.0717	0.0292	0.0000	0.0466	−69.38	150.77	0.30

ARD, all rates different; ER, equal rates; SYM, symmetric rates.

Table S2. Model-averaged transition rates between dietary states

State	1	2	3
1	—	0.03	0.0
2	0.05	—	0.04
3	0.00	0.05	—

1, hypercarnivory state; 2, mesocarnivory state; 3, hypocarnivory state.

Table S3. Variable loadings on the three linear discriminant (LD) functions used to classify fossil canids to dietary regimes, and the strength and significance of their correlations with RLGA

Trait	LD1	LD2	LD3	r^2	*P* value
RBL	−45.49	1.35	−31.12	0.88	<0.001
M1BS	1.48	1.70	79.09	0.86	<0.001
M2S	−3.32	12.75	−4.74	0.93	<0.001
MAT	24.71	−8.26	13.08	0.36	<0.001
p4S	−9.92	−15.26	−6.59	0.69	<0.001

MAT, moment arm of temporalis; M1BS, lower first molar blade size (relative to jaw length); M2S, relative size of upper second molar; p4S, shape of lower first premolar; RBL, relative length of the m1 blade.